32nd EUROKIN CONSORTIUM WORKSHOP

EXTENDED ABSTRACT

The Random Corrugated Pore Structure Model

Work prepared by

Dr C.E. Salmas and
Prof. G.P. Androutsopoulos

School of Chemical Engineering
National Technical University of Athens

University of DELFT (The Netherlands)
14 16 February 2012

EXTENDED ABSTRACT

Introduction

The present work concerns the application of experimental methods and theoretical models focusing on the study of the physical porous structure of solids catalysts as well as of a wide variety of nano-structured porous materials like adsorbents, membranes, filters bio-materials etc. Such materials may exhibit random or regular hierarchical pore structures and the principal interest is directed to the reliable determination of fundamental properties like the specific pore surface area,(S_g), the pore size distribution (PSD) referring to either the pore volume, or the surface area and or even the pore population. These properties represent a kind of identity of a material and provide the frame to model and further investigate physical, fluid mechanical and chemical processes occurring on or within these solids.

Pore structure properties evaluation is achieved via the theoretical processing of the pertinent experimental data obtained by applying methods like: (1) gas Physical Sorption especially at low temperature (ca. at the normal boiling point of the gas being used) [1,2], (2) Mercury Porosimetry [1] (i.e. mercury intrusion (penetration) into the evacuated pore space of the material by a stepwise increase of an externally applied pressure, $\Delta P>0$, up to a maximum (e.g. 200-300 MPa). The reverse experiment involves mercury retraction, caused by the capillary forces action, when the external pressure is being decreased stepwise, $\Delta P<0$) and (3) Electron Microscopy Methods (e.g. SEM, TEM etc) that enable the application of extremely high pore size magnification thus offering the advantage of immediate observation of pore shape, surface texture and chemistry. However a big number of images is required to obtain an overall representative picture of the pore structure and surface features of the studied material. Pore microphotographs however should be considered as quite valuable independent information supplementing porosimeter measurements.

The extend of S_g, and the PSD characteristics of a catalytic substrate play a controlling role in conjunction with other factors regarding the intrinsic catalyst reactivity, diffusion of reactants into and products out of a catalyst pellet, [4, 5]. A characteristic example is the interaction between pore size and reacting macromolecules e.g. asphaltenes during the catalytic hydroprocessing of liquid fuels fractions, [6].The knowledge of the PSD and the establishment of a physical pore structure model are the necessary tools to investigate catalyst deactivation and regeneration phenomena due to the carbon by-product lay down during the catalytic hydroprocessing of hydrocarbons, [7, 8].

Contemporary Nitrogen and Mercury porosimeters are supplied with computer software for routine immediate processing of the raw experimental measurements to deduce pore surface areas S_g, (e.g. BET, [10]) and PSDs, (e.g. BJH, [9]). The use of the conventional calculation packages have been established long ago and are widely accepted because of their simple structure and the speed with which they generate results. However it should not escape our attention that potential users for routine analysis do not care much for high accuracy of pore structure properties measurements but are mostly interested to assess the change of these properties for a family of samples that had been subjected to well known processing conditions. It may be also true that the users can not have an immediate access or they do not trust the new advanced methods of pore structure characterization.

The conventional techniques e.g. the BJH or similar like the Roberts, Cranston-Inkley, Modeless, etc, [1] and new ones e.g. the DFT, (Density Functional Theory [2, 11]), present the drawback that the calculation of pore properties relies separately either on gas adsorption-capillary condensation or desorption–capillary evaporation data and usually predict quite differing results. The controversy as to whether the condensation or the evaporation data are more appropriate is a long standing one. By selecting one

branch of the hysteresis loop or the other seems like ignoring hysteresis loop as a whole and the phenomena causing it. e. g. pore networking and/or thermodynamic metastability. In contrast such phenomena are taken into account in the formulation of the CPSM model under consideration and their impact is reflected in the CPSM predictions.

In the present work an attempt is done for a concise review of the principles and applications of the unified theory of the CPSM model (Corrugated Pore Structure Model [6, 12, 13] that is transformed into an integrated computation model simulating the hysteresis phenomena associated with Nitrogen Sorption (CPSM-N_2) [14-17] and mercury porosimetry (CPSM-Hg) [12] measurements. A list of several relevant publications is given to serve as the source of additional information.

The CPSM-RS, [16] enables the determination of intrinsic PSD [12, 13] the true pore surface area S_{CPSM} via the integration of the pore surface area PSD by taking account of pore curvature an element that is ignored in the multilayer BET method and can lead to surface area S_g predictions reduced by a percentage >30% compared to the corresponding S_{CPSM} values in cases where the material possess pore sizes, D_p<4 nm. [18]. CPSM-RS, predicts also values $S_{CPSM(fs)}$ comparable to the corresponding BET values if pore curvature will be ignored

Moreover the CPSM-N_2 provides the capacity of evaluating pore structure tortuosity, τ_{CPSM} ,and the effective diffusion coefficient D_{eff} , [19], the determination of microporosity (D_{pore}<2 nm), [15, 19, 20] and the prediction of catalyst pore structure and carbon deposits interactions.[6, 7].

Theory

CPSM-physical representation; Various literature pore structure models provide an idealized picture of the structure exhibited in real porous material, are shown in Fig. 1(a). The two and three-dimensional models are configurations resembling closer the structure of real materials. Nevertheless the less they include additional parameters that have to be determined and verified experimentally. The CPSM model represents a mere modification of the well known 'bundle of independent cylindrical pores of distributed size' comprising a set of 'independent corrugated pores' where each one is composed of a series of Ns cylindrical segments distributed in size.

FIGURE 1
FIGURE 2

Parameter N_s is defined as the nominal pore length and is actually the frequency of pore cross-section area variation and can considered as being the measure of 'networking effect' and as such is introduced in the empirical eq. (1) that predicts tortuosity factors by exploiting nitrogen sorption data subjected to a CPSM analysis [21].

$$\tau_{CPSM} = 1 + 0.69 \left[\left(D_{max,eff} - D_{min,eff} \right) / D_{mV} \right] \left(N_S - 2 \right)^{0.58} \quad (1)$$

CPSM-Nitrogen. Regarding the simulation of gas adsorption/desorption the formulation of the CPSM model was based on the probabilistic analysis of the following phenomena: (i) gas adsorption / desorption as it is expressed in a modified Halsey correlation, eq. (2) (the conventional Halsey is deduced from eq.(2) for n=0.35 and m=0), and (ii) capillary condensation/evaporation according to the Kelvin equation (eq.3) in the frame of a

$$t = n \left[5 / ln \left(P_0 / P \right) \right]^{1/3} \left(P / P_0 \right)^m \quad (2)$$

$$D_K = \left[1.906 / ln \left(P_0 / P \right) \right] cos\theta \quad (3)$$

representative corrugated pore. Equation (3) is valid for a hemispherical geometry of the liquid /gas (l/g) interface geometry when ($\cos\theta \equiv \cos\theta_h = 1$ and cylindrical when $\cos\theta \equiv$

$\cos\theta_c$ = 0.5 and the numerator is evaluated from the formula $(2V_L\gamma/RT)=1.906$ where $V_L=34.517$ cm^3/gmol, γ=8.88 mN/m, R=1.987 cal/(gmol K), T=77.35 K and $[D_K]$=nm.

$$V_{ads} = \left[1 / \int_{D_{min}}^{D_{max}} D^2 F(D)dD \right] \left[4t \int_{D_h}^{D_{max}} (D-t)F(D)dD + \int_{D_{min}}^{D_C} D^2 F(D)dD + \right.$$

$$\left. + \int_{D_C}^{D_h} D^2 F(D)dD \left(\frac{1}{N_S} \sum_{j=1}^{j=Ns} \left(P_j \right) \right) + 4t \int_{D_C}^{D_h} (D-t) F(D)dD \left(\frac{1}{N_S} \sum_{j=1}^{j=Ns} (1-P_j) \right) \right] \quad (4)$$

$$V_{sr} = 1 - \int_{D_h}^{D_{max}} (D-2t)^2 F(D)dD \left(\frac{2}{N_s} \frac{1-q^{N_s}}{1-q} - q^{N_s} - 1 \right) \Bigg/ \int_{D_{min}}^{D_{max}} D^2 F(D)dD \quad (5)$$

The formulation of mathematical relations concerning the adsorption/capillary condensation process according to CPSM-N_2, i.e. eq. (4) and the desorption/capillary evaporation, eq. (5) requires the definition and synthesis of the basic probabilistic events that control: (1) the metastability phenomena, i.e. the variability of the l/g interface geometry, occurring during the adsorption and capillary condensation stage and (2) the networking effect imposed by the corrugated pore irregular structure during the desorption/evaporation process, [13].
The authors of the present study formulated and are using systematically as intrinsic pore size distribution F(D) (eq. 4-8) the home made QE distribution (formerly called BSD) and illustrated in Fig. 2(b). The analytical formula is provided in eq. (6).

$$F(D) = [(D - D_{min})\ (D - D_{max})\ exp(-bD)] / \Phi(D) \quad (6)$$

where Φ(D) is the normalization factor

This single parameter distribution can be integrated analytically and apart from the achieved high accuracy of calculations imparts its own contribution in reducing the computation time requirements associated with the various CPSM applications encountered in gas sorption and mercury porosimetry.

CPSM-RS*:* It becomes obvious from Fig. 3 (a) that a specified number of nitrogen atoms, assumed to be rigid spheres, occupy fully the internal cylindrical surface of an imaginary pore. Besides they cover only part of an equal flat surface. This outcome is obvious since in the first case a single molecule 'shadows' an elliptical fraction of the cylindrical surface that is higher than the respective circular molecular imprint on the plane surface, Fig. 3(b). In Fig. 3(c) the relative error in assessing the pore surface area if pore curvature is ignored is plotted against the pore size. It is clear from the latter plot that an error of 15-35% may be encountered for pore structures ranging from 2-4 nm. Most of the MCM-41 and similar materials possess such a structure. More details on this subject are reported in [16].

FIGURE 3.

CPSM-Hg: The development of the CPSM-Hg equations i.e. MP (branch P) eq. (7) and MP (branch R) eq.(8) follows a procedure similar to that applied in the formulation of CPSM-N2. The prediction of the hysteresis loop is attributed to various factors: (1) the pore networking effect during intrusion and extrusion, (2) The change of the Hg-solid contact angle between mercury intrusion and extrusion (i.e. contact angle hysteresis) and

(3) the mercury entrapment phenomenon during mercury withdrawal that it is supposed to result from mercury column 'snap off' occurring when a mercury retreating meniscus, under reducing pressure conditions, is going to pass through an abrupt cross section reduction where the 'pore constriction ratio' $\lambda = D_{p\,(i+1)} / D_{pi}$ is less than an acceptable limiting value, e.g $\lambda<0.66$.

$$V_P\left(P(D)\right) = \frac{A}{k}\left(\int_{D}^{D_{max}} D^2 F(D)dD \Big/ \int_{D_{min}}^{D_{max}} D^2 F(D)dD \right) \tag{7}$$

where $A=(1-P_S^{2k})/(1-P_S)-kP_S^{2k-1}$ *for* $P_S<1$ *or* $A=k$ *for* $P_S=1$ *and* $P_S = \int_{D}^{D_{max}} F(D)dD$

Case (i): for $D_{min}<D<(D_{min}/\lambda)$ $\quad V_W\left(P(D)\right) = \left(\frac{B}{2k^2} \Big/ \int_{D_{min}}^{D_{max}} D^2 F(D)dD \right) \int_{D_{min}}^{D} D^2 F(D)dD$

Case (ii): for $(D_{min}/\lambda<D<D_{max}$

$$V_W\left(P(D)\right) = \left(\frac{B}{2k^2} \Big/ \int_{D_{min}}^{D_{max}} D^2 F(D)dD \right) \left[\int_{D_{min}/\lambda}^{D} \left(D^2 F(D) \int_{D}^{D_{max}} F(D)dD \right) dD + \int_{D_{min}}^{D_{min}/\lambda} D^2 F(D)dD \right] \tag{8}$$

- ***Contact angle hysteresis:*** A comparative application of the CPSM-N_2 and CPSM-Hg on nitrogen sorption and mercury porosimeter data for anodic alumina foil yielded the result depicted in Fig. 4. It should be noted that both methods predicted the same intrinsic PSD and the fact that satisfactory regression of the mercury porosimetry data became possible by using contact angles θ_p =143º and θ_r=102º. A thorough presentation on the subject is reported in [22].

FIGURE 4.

- ***Pore Structure Tomography of Meso-macroporous Materials***

  (Hysteresis Loop Scanning)

From the curve fitting of MP hysteresis loop data scanning along each one of the experimental lines forming the MP hysteresis loop the relevant tomography intrinsic PSD data were generated. Such data provide pore structure information for parts of the structure independently. A full account of the theory and applications on MP tomography as relates to CPSM are reported in [12].

FIGUREC 5.

- **Catalyst Deactivation; Pore Structure and Carbon Foulant Interactions**

Catalyst deactivation due to coking (i.e. carbonaceous by-products formation and deposition on the catalyst surface during petroleum processing) is an undesired situation with considerable economic implications. The corrugated pore configuration (originally named 'series' pore, [25]) was selected to study pore structure and coke interactions. The theoretical analysis demonstrated that a non-uniform coke deposit thickness occurs along a catalyst pore even when reactants diffusion limitations are not present (Fig. 6(a) [25]). This is the result of gradual plugging of pore constrictions by coke depositions of increasing thickness from pore center to mouth, letting behind halve filled pore segments and still active surface area though becoming inaccessible to reactants. The now named CPSM-Deactivation Model [25] is employed in parametric studies illustrating the pore length (parameter j) impact on the curves relating the amount of accumulated coke vs its layer thickness, Fig. 6(b). This same model was also successfully applied to curve fit experimental coke deposits vs coke layer thickness data obtained during Greek oil residue catalytic hydrodesulphurization experimentation, Fig. 6(c), [7, 26].

FIGURE 6.

- **Anodic Alumina Oxide Membrane Characterization. A Recent CPSM-Nitrogen Model Application**

Anodic oxidation of aluminum tube in sulfuric acid achieved the formation of membranes exhibiting regular mesoporous structures of open ended independent pores to enable the perselective separation of hydrogen from mixtures with other synthesis gas components, Fig. 7(a) [27]. The application of the CPSM-Nitrogen enables the systematic study of membrane pore structure obtained under differing anodization conditions e.g. anodization time, current density, etc, as well as pore structure variation following chemical and hydrothermal treatments, Fig. 7(b). More important is the evaluation of tortuosity values τ_{CPSM} values that contributed in the definition and calculation of a novel dual Knudsen number (i.e. based on pore structure properties) that is consistent with the Knudsen Number obtained from single gas per-selectivity measurements, [27].

FIGURE 7,

Concluding Remarks

The Corrugated Pore Structure Model (CPSM) is based on a 'composite cylindrical pore configuration', is a unified theory and a flexible computer code employed in the characterization of porous solids via the simulation of gas sorption and mercury porosimetry hysteresis data. It uniquely predicts intrinsic pore size distributions (ca. referred to volume, surface and population) over the entire macro- to micro- pore size range. The CPSM-R.S Rigid Spheres variant predicts, through the integration of the surface area distribution, true total pore surface areas by taking account of pore curvature and if curvature is ignored moderate surface areas, closer to BET values, are obtained. The CPSM theory enables the evaluation of pore structure tortuosity factors that are related to catalyst effective diffusivity evaluations.

The CPSM-Mercury Model, in addition to simulating the overall hysteresis loop, is transformed and adjusted to represent the PR Hysteresis loop scanning either along the penetration branch or the retraction line. The latter is less significant since only part of the pore system is involved in the retraction process due to mercury entrapment. However, if the distribution of the entrapped mercury is predicted, retraction lines free of entrapment can be constructed and the related pore size distributions can thereby be deduced.

CPSM-Deactivation is a theoretical model accompanied by a computer code dealing with distribution of carbon (coke) deposits accumulated along an assumed corrugated pore structure. Its comparison with experimental data offers useful insights of pore structure –coke deposit interactions.

Extensive use of CPSM-Model variants is included in ref. [23] (CPSM-Hg) and in ref. [18, 24] (CPSM-N_2 or CPSM-R.S). Development work is continued on applications of optimized computer software involving both methods of pore structure characterization and ensuring a reliable, user friendly performance for widespread applications.

Literature

[1] S.J Gregg, K.S.W. Sing Adsorption, Surface Area and Porosity, 2nd Ed, Academic Press, (1982) London.
[2] F. Rouquerol, J. Rouquerol, K. Sing, Adsorption by powders and porous solids, Academic Press, (1999) London.
[3] G.E.Thompson, R.C. Furneaux., G.C. Wood, Corros. Sci., 18, (1978) 481.
[4] A. Wheeler, *Reaction Rates and Selectivity in Catalyst Pores*. 'Catalysis' Vol. II, Reinohold, New York. 1955.
[5] C.N Satterfield, *Mass transfer in heterogeneous catalysis*, M.I.T. Press, London, 1970.
[6] G.P.Androutsopoulos, R.Mann, Chem. Eng. Sci., 34, (1979) 1203.
[7] J.M.Ammus, G.P.Androutsopoulos, A.H.Tsetsekou, Ind. Eng. Chem. Res., (i) 26,.(1987) 494-501, (ii) 26, (1987) 1312
[8] M. Sahimi, G.R. Gavalas, T.T. Tsotsis, Chem. Eng. Sci., 45, (1990)1443.
[9] L.P. Barrett, L.G. Joyner, P.P. Halenda, Am. Chem. Soc., 73, (1951) 373.
[10] S. Brunauer, P.H. Emmett, E. Teller, J. Am. Chem. Soc., 60, (1938) 309.
[11] P.I. Ravikovitch, G.L. Haller, A.V. Neimark, Adv. Colloid Interface Sci., 76-77, (1998) 203.
[12] G..P Androutsopoulos, C.E., Salmas, Chem. Eng. Commun., (i) 176, (1999),1, (ii) Part 1, 181 (2000) 137, (iii) Part 2, 181 (2000) 179.
[13] G.P Androutsopoulos, C.E., Salmas, Ind. Eng, Chem. Res., (i) Part I 39 (2000) 3747, (ii) Part II 39 (2000) 3764.
[14] C.E. Salmas, V.N. Stathopoulos, P.J. Pomonis, G.P Androutsopoulos, Langmuir, 18 (2000) 423.
[15] C.E. Salmas, A.K. Landavos, S.P. Skaribas, P.J. Pomonis, G.P Androutsopoulos, Langmuir 19 (2003) 8777.
[16] C.E. Salmas, G.P Androutsopoulos, Langmuir, 21(24), (2005) 11146.
[17] C.E. Salmas, G.P Androutsopoulos, Applied Catalysis A: General, 210 (2001) 329.
[18] P. Kowalczyk, et al., J. Colloid Interface Sci., 297, (2006) 77.
[19] C.E. Salmas, et al, Applied Catalysis A: General 216 (2001) 23.
[20] C.E. Salmas, G.P Androutsopoulos, Chem. Eng. Commun., 196 (2009) 407–442.
[21] C.E. Salmas, G.P Androutsopoulos, Ind. Eng. Chem. Res., 40 (2001) 721.
[22] C.E. Salmas, G.P Androutsopoulos, J. Colloid Interface Sci., 239 (2001) 178.
[23] F. Moro, H., Böhni, J. Colloid Interface Sci, 246, (2002) 135.
[24] S.Furmaniak, A.Terzyk, P. Gauden, G. Rychlicki, J. Colloid Interface Sci., 295, (2006) 310.
[25] G.P. Androutsopoulos, R. Mann, Chem. Eng. Sci., 33 (1978) 673-682.
[26] E. Furimsky, F. E. Massoth, Catalysis Today 52 (1999) 381-495
[27] S. Th. Vaitsi, C.E. Salmas, O.G. Tsapekis, A.P. Katsoulidis, G.P. Androutsopoulos, Fuel Processing Technology 92 (2011) 2375–2388.

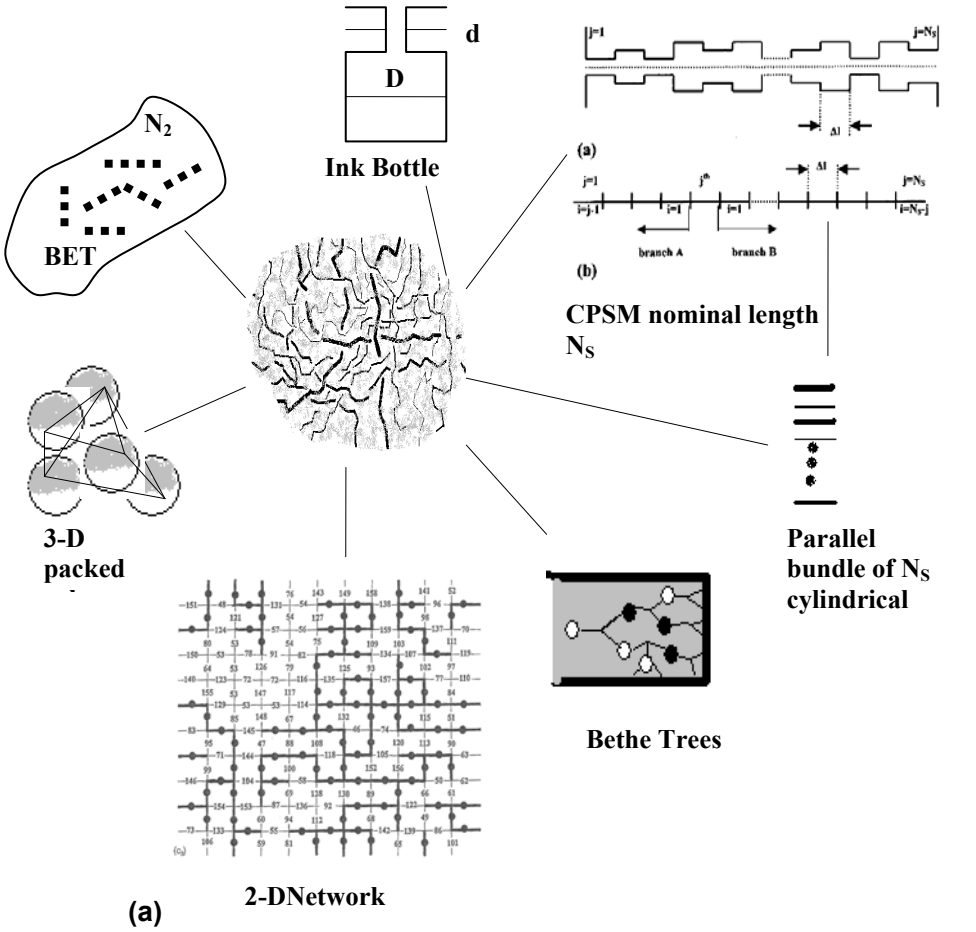

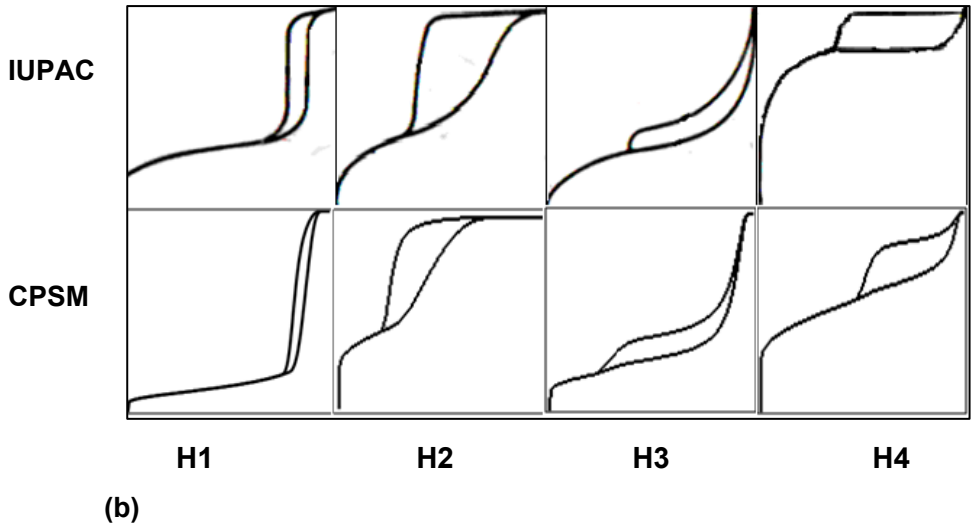

Fig. 1 **(a)** Pore Structure models representing the pore structure of porous materials **(b)** Gas sorption hysteresis loops according to the IUPAC classification (upper row) and to the CPSM model (lower row) [13, part I],

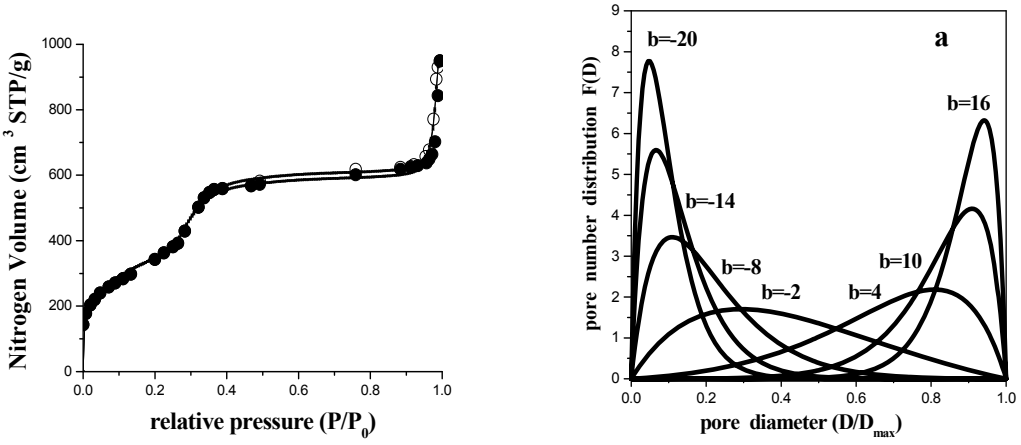

(a) **(b)**

Fig. 2 **(a)** CPSM data fitting of Nitrogen Sorption Isotherms of an MCM-41 mesoporous material exhibiting regular pore structure and **(b)** The QE (Quantratic- Exponential) distribution, eq. (6).**,** [13, i].

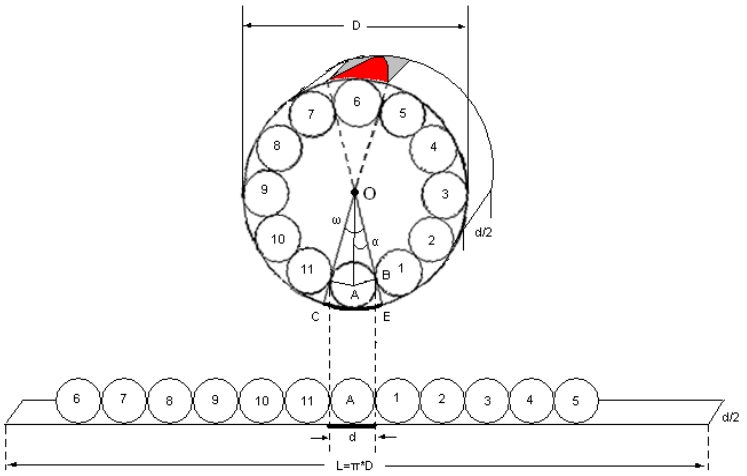

Fig. 3 (a)

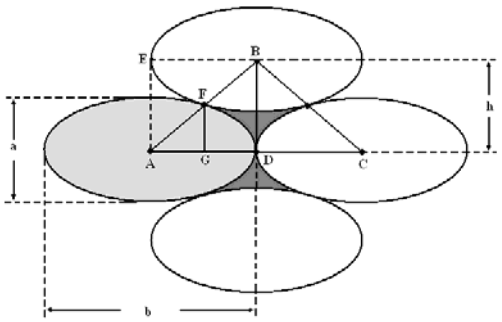

Fig. 3(b)

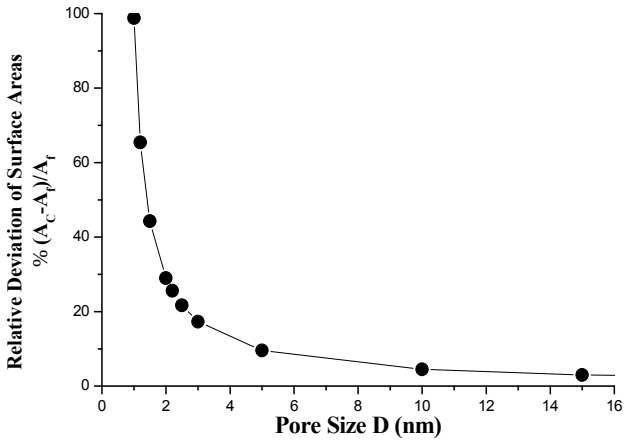

Fig. 3(c)

Fig. 3 Effect of Pore Curvature in the evaluation of Pore Surface Area

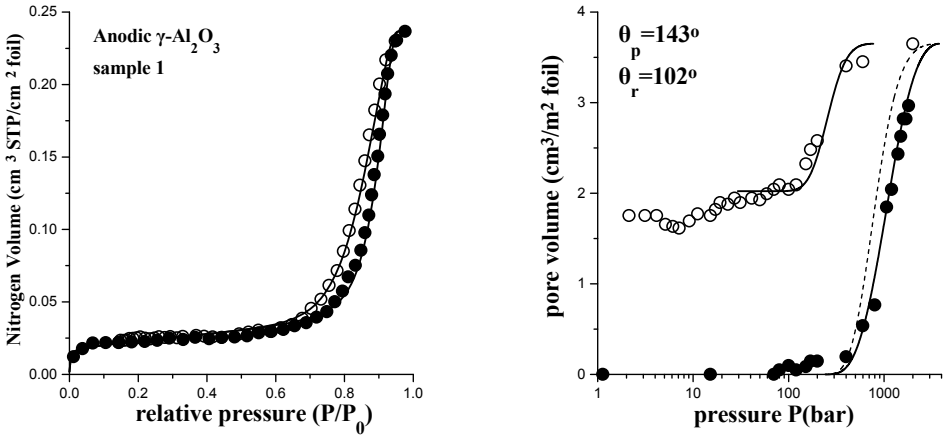

(a) **(b)**

Fig. 4. CPSM fitting on anodic alumina data points: (a) Nitrogen sorption at (-196.67 ºC) and (b) Mercury porosimetry hysteresis data.

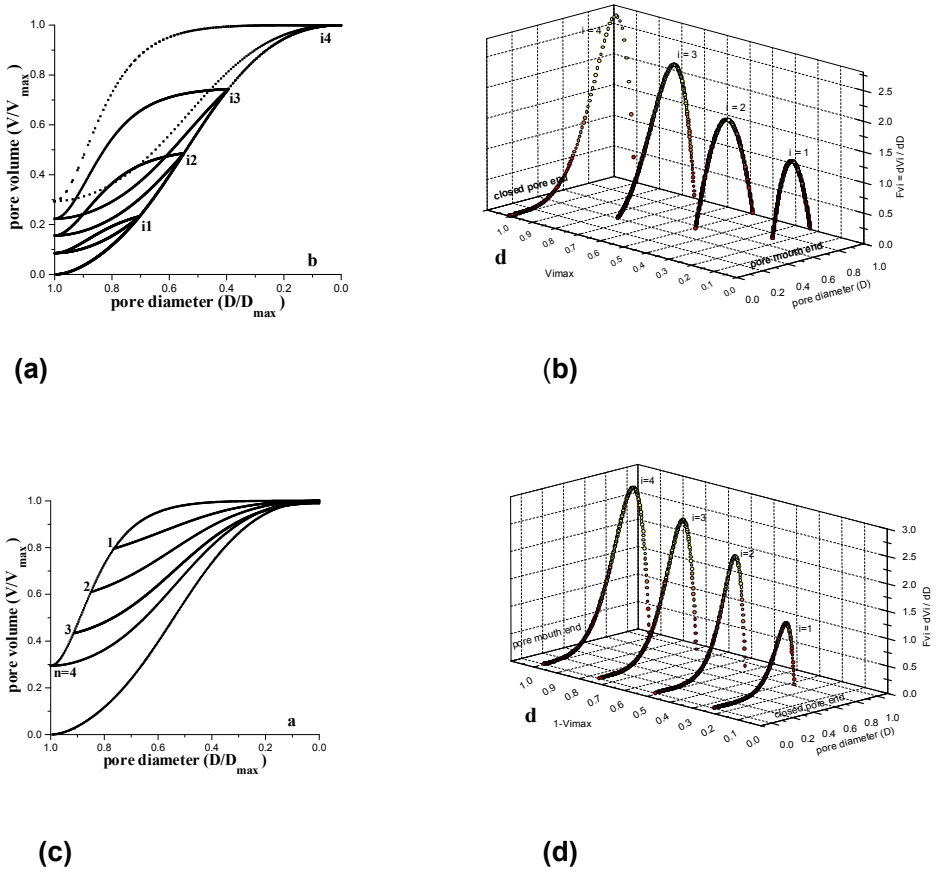

Fig. 5. Loop scanning of mercury porosimetry hysteresis loops and the corresponding tomography PSD spectrum: (a, b) scanning along the mercury intrusion branch [12 ii] and (c, d) scanning along the mercury extrusion hysteresis branch [12 iii].

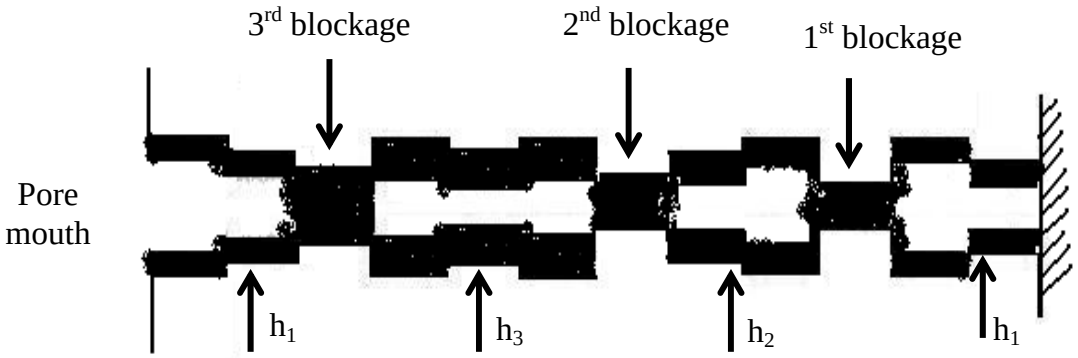

Carbon deposit thickness = $h_1 < h_2 < h_3$

Fig. 6 (a) [25]

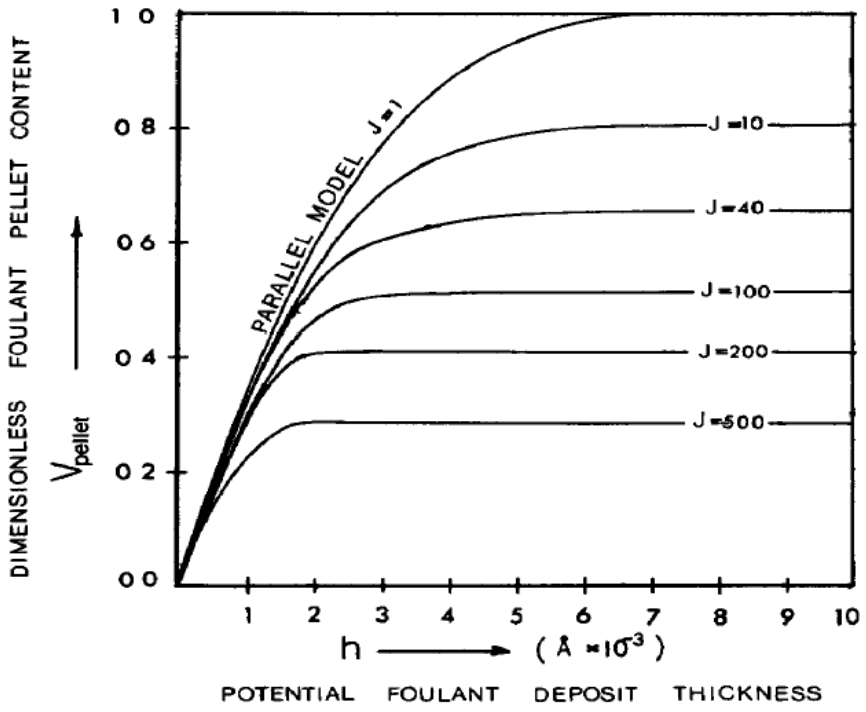

Fig. 6(b) [25]

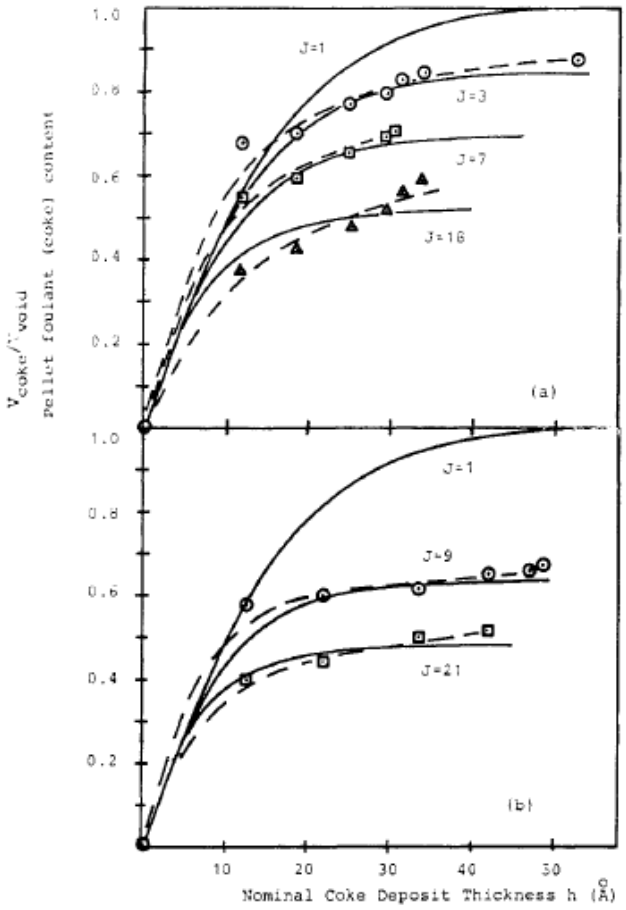

Fig. 6(c) **[7]**

Fig. 6 Catalyst deactivation by pore plugging by coke deposition: (a) Non-uniform coke deposition along a corrugated pore, (b) Theoretical relative carbon foulant content vs coke thickness, [25], (c) Regression result of the CPSM-deactivation model over experimental relative coke pore deposit vs the nominal coke deposit thickness, [7].

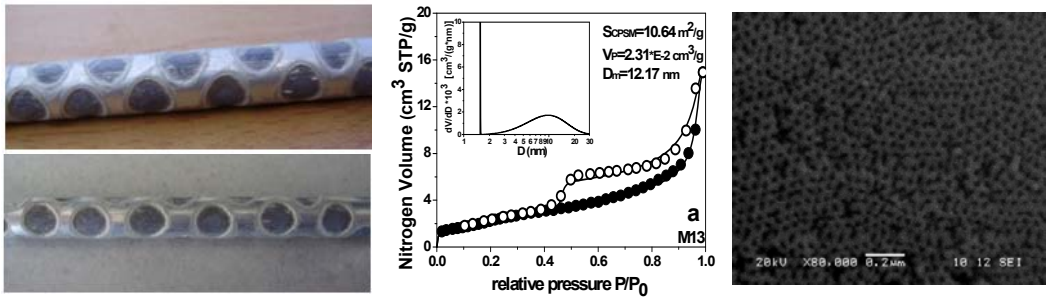

Robust spotted pattern anodic alumina membranes

Mesopore size anodic alumina membranes

Independent regular pores of ~5.6E+14 pores/m^2.

Fig. (7) (a) GRAPHICAL ABSTRACT [27]

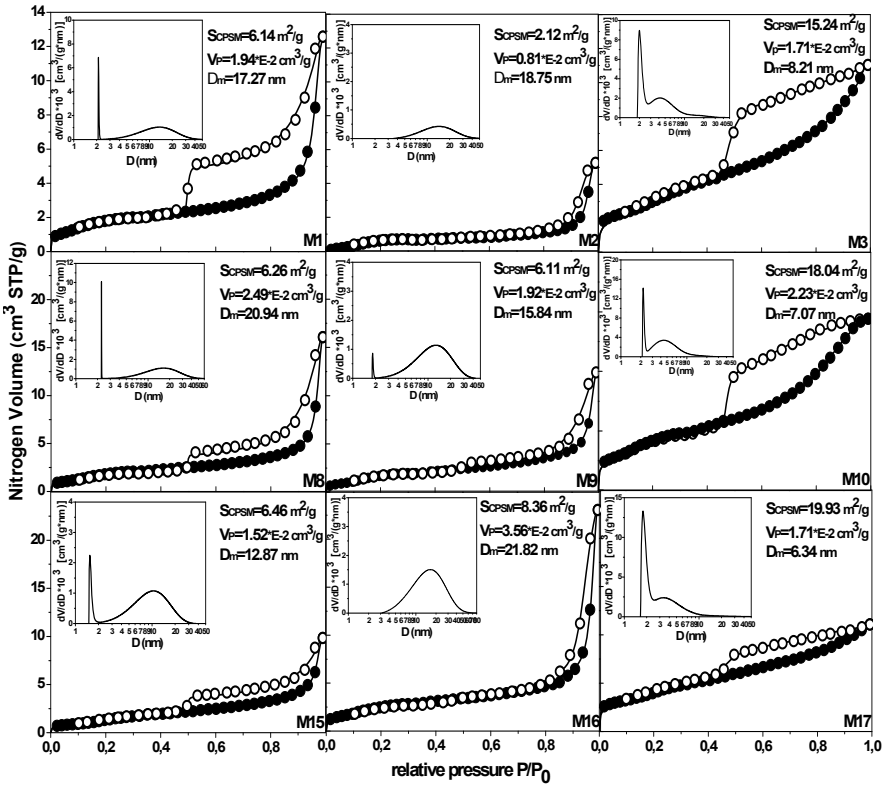

(b) [27]

Fig. 7 Anodic Aluminum Oxide Membrane: (a) view of external spotted pattern, nitrogen sorption hysteresis loop, SEM image depicting the regular arrangement of pore entrances, (b) Effect of chemical and hydrothermal treatments on nitrogen sorption.characteristics. M1, M8, M15 anodization only, M2, M9, M16 combined anodization and chemical etching, M3, M10, M17 combined anodization with chemical and hydrothermal treatments. The respective pore volume distribution, mean pore size, pore volume, specific surface area (S_{CPSM}) are provided as insets (plot and text). [27].